

# Numerical Study on the Crushing Behavior of Square Tubes Under Three Dimensional Oblique Loading

A. Khalkhali\*, M. Sarmadi, A. Bodaghi

Automotive Simulation and Optimal Design Research Laboratory, School of Automotive Engineering, Iran University of Science and Technology, Tehran, Iran

\*Corresponding Author

## Abstract

This study aims to numerically investigate on the crashworthiness of thin-walled square tubes by consideration of 3-D oblique loading. In this type of loading, direction of loading is defined by using two spatial angles relative to the position of the tube. To this aim, finite element (FE) analysis is employed to simulate the loading for 8 different numerical models with different loading orientation. Subsequently, load-displacement diagrams as well as deformation shapes during the loading are derived for each model. Moreover, a study is done on the tube collapse mode for each case. Effect of loading orientation and tube thickness on the maximum crushing load and energy absorption are also studied via a parametric study on the FE simulations. Results indicated a different trend for all cases of 3D oblique loading compared to axial loading. This study highlights the significance of consideration of a 3D orientation in analysis of crushing behavior of thin-walled tubes.

**Keywords:** Energy absorption, Three-dimensional oblique loading, Thin-walled square tube, Quasi-static crushing behavior, Collapse mode, ABAQUS/Explicit

## 1. Introduction

Thin-walled square tubes are widely considered as one of the energy absorbers with low weight and considerable crashworthiness capabilities. Crashworthiness of such structures have been investigated in many studies under axial loading [1-5]. However, in actual crash events, energy absorber structures are more likely under oblique loading.

Some researchers have studied crashworthiness characteristics of thin-walled tubes under oblique loading in previous works. Han et al. [6] for the first time studied the crushing behavior of thin-walled square tubes under oblique loading using LS-DYNA. They showed through numerical study that there is a critical load angle at which a transition takes place from the axial collapse mode to the bending collapse mode. Reyes et al. [7, 8] experimentally and numerically investigated the behavior of square aluminum tubes under quasi-static oblique loading for three different load angles. The square tubes were clamped at one end and oblique loading conditions were realized by applying a force in the upper end, with different angles, relative to the centerline of the tube. Yang et al. [9], using nonlinear finite element analysis through LS-DYNA, investigated the crushing behavior a class of axisymmetric thin-walled square

tubes with two types of straight and tapered geometries and two forms of cross-sections (single-cell and multi-cell) as energy absorber components under oblique impact loading.

In all of conducted researches, oblique load was defined by one angular parameter in a 2D coordinate system. However, in real crash events, loading has a 3D spatial direction. Thus, the load can be considered as a 3D oblique load.

In this study, a numerical approach is employed to study 3D oblique loading imposed on a thin walled structure with square section. The main purpose of this study is to 1) study on general deformation and local plastic collapse of the tubes, 2) derivation of load-displacement diagram. To this aim, FE simulations using ABAQUS in accordance with experimental conditions are accomplished. Results obtained from FE simulations are then used for the parametric study. Numerical simulations along with parametric analysis indicated interesting results that can be used for design of thin-walled energy absorber structures, with articular usage in automotive industry.

## 2. Finite-element modeling

In the present study, FE simulations were done using commercial software Abaqus/Explicit. Obtained results have been later used for parametric study. In

all simulations, 4-node doubly curved thin shell element (S4R), which is appropriate for large strain analysis, was used. To model the bending effect, five integration points were used through the shell thickness. Mechanical behavior of the constitutive material was considered according to the results of tensile test for stainless steel grade 201. The plastic behavior was also defined based on stress-strain graph. In the FE analysis, the upper cross-head was modeled as a rigid plate, and all of its degrees of freedom except displacement along load direction were constrained. The models were completely tied to the rigid plate in the upper end.

In the FE analysis, the upper cross-head was modeled as a rigid plate, and all of its degrees of freedom except displacement along load direction were constrained. The models were completely tied in to the rigid plate the upper end. To reduce the time step, the velocity of the upper rigid plate was considered equal to 0.1 m/s. Moreover, the Amplitude option and SMOOTH STEP sub option in ABAQUS/Explicit were used to control the velocity to ensure a valid quasi-static analysis [10-13]. The

lower plate was configured based on angles of  $\theta_1$  and  $\theta_2$ . This plate was also modeled as a rigid plate during simulations. As observed in Fig. 1, position of the inclined lower plate is defined by two angles,  $\theta_1$ , the angle of the plate rotation along the vertical axis, passing through the centroid of cross-head, and  $\theta_2$ , the angle of the plate relative to the horizon. by rotating the upper circular plate relative to the lower one,  $\theta_1$  is changed, and by rotating the declined plate relative to the upper circular plate,  $\theta_2$  is changed. Numerical simulations for 8 different numerical models of thin-walled tubes were performed. Characteristics of the models as well as the loading conditions for each model is depicted in Table 1, where C is the thickness, and L is the length of the tubes.

A comparison between kinetic and internal energy of the numerical models also showed that due to quasi-static loading conditions, the amount of kinetic energy was rather negligible, which represented the validity of the performed quasi-static conditions. Friction coefficient of 0.3 was considered for the contact between the tube and rigid plate.

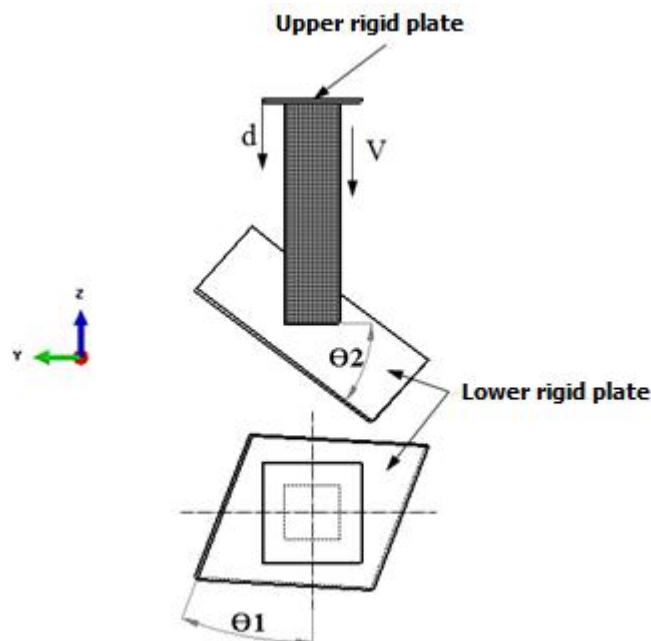
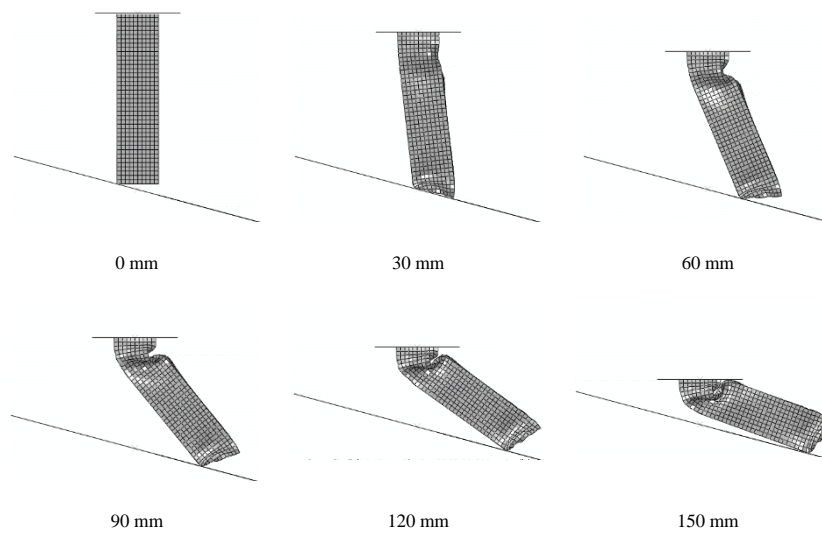


Fig1. Definition of  $\theta_1$  and  $\theta_2$  in numerical simulations.

**Table 1.** Geometrical and loading properties of numerical test models

Test No.	C (mm)	L(mm)	Thickness(mm)	$\theta_1$ (deg)	$\theta_2$ (deg)
A1				0	15
A2				0	25
A3				0	30
A4	50	200	1.6	0	35
A5				15	25
A6				15	30
A7				15	35
A8				30	35



**Fig2.** Deformation of the numerical model A1 for different cross-head displacements

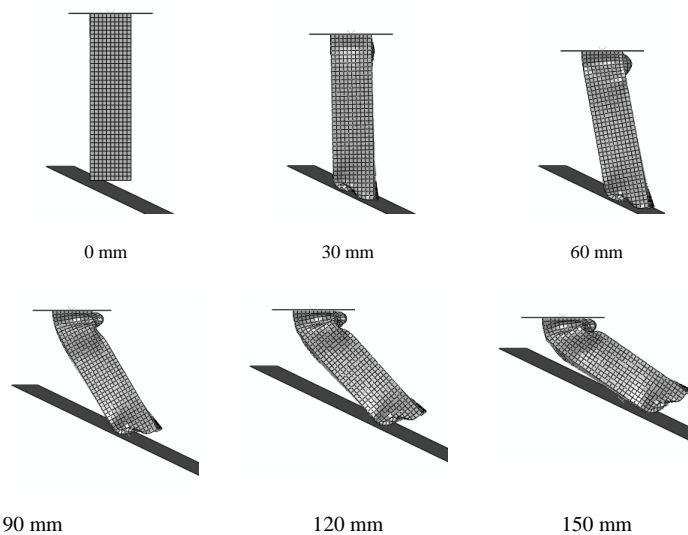


**Fig3.** Deformation of the numerical model A5 for different cross-head displacements

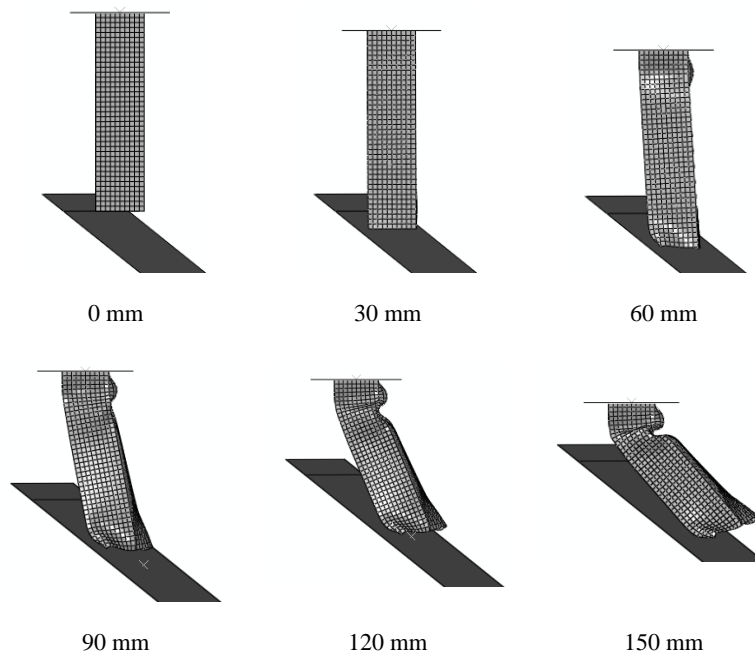


Fig4. Deformation of the numerical model A8 for different cross-head displacements

### 3. Results

Accordingly, Figs. 2 to 4 show the plastic deformation of models in numerical studies when the cross-head displacement is 0, 30, 60, 90, 120 and 150 mm. Deformation shape and load-displacement diagram considering the first peak load (F1), maximum crushing load (Fmax) as well as energy absorption (Eabsorp.) are presented Fig. 5, where parameter C is equal to 50 mm for all models. Evidently, effect of the oblique loading by changing  $\theta_1$  and  $\theta_2$  is completely visible. It is observed that these angles can have a dominant effect on the trend of diagrams in all simulations. Based on Figs. 2 to 4, the present numerical model is very accurately capable of capturing plastic folding, as well as deformation in contact interface between the lower rigid plate and the tubes.

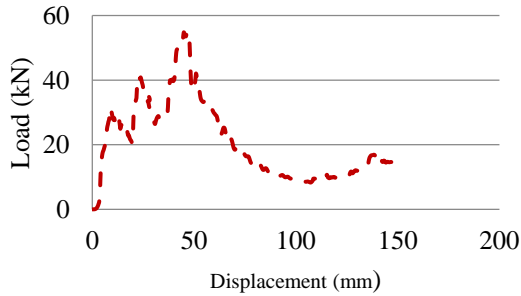
As presented in Fig. 5, the crush load in all graphs has an ascending trend after the highest peak. Notably, these graphs are entirely different from the conventional load-displacement graph of the crushing behavior of a thin-walled tube under axial loading. Under axial loading conditions, as the cross-head displacement increases, the load reaches a peak value thereafter it continues by a series of fluctuations with lower peaks. However, under 3D oblique loading, there is a subsequent higher peak after the initial one, for larger  $\theta_2$  such as one in A7 (with  $\theta_2=35^\circ$ ), the dominant mode becomes the bending mode, however,

F1. This secondary peak load, which is the highest amount of applied load, is considered as the maximum peak crush load in the present paper or Fmax. Notably, as the angles of the declined plate approach to 0, the load-displacement trend becomes more similar to the axial loading condition. Fig. 5 indicates that in initial contact between models and the declined plate, tube section has not entirely undergone in contact with the declined plate, and therefore, the load has been applied fully on the interface between the tube and the plate. This condition leads to local collapse of the tube, and the load that results in the first local collapse is equal to the first peak crush load (F1). This load depends on the interface area which changes according to  $\theta_1$  and  $\theta_2$ . By increasing the cross-head displacement, when the whole tube section undergoes in contact with the declined plate, the remained part of the tube shows the crushing behavior similar to axial loading conditions on a relatively flat support. Under this condition, the load that creates the first folding in the tube is the maximum peak crush load or Fmax.

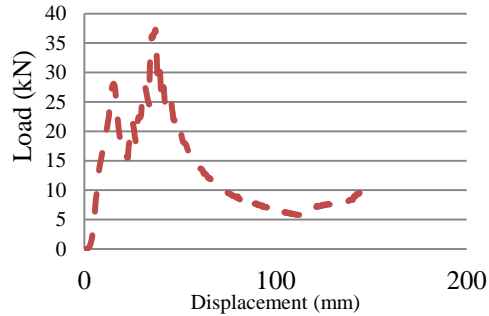
Based on investigations in [7], the dominant collapse mode in oblique loading condition is expected to be the bending mode. However, numerical observations of this paper show that the collapse mode is a combination of bending, torsional and axial (or progressive buckling) modes. Notably

in other cases it remains the axial mode. This contradiction can be attributed to the boundary conditions of one end of the models which undergoes

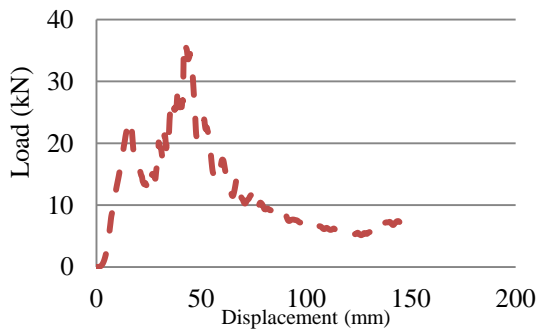
the oblique loading. In conducted experiments in reference [7],.



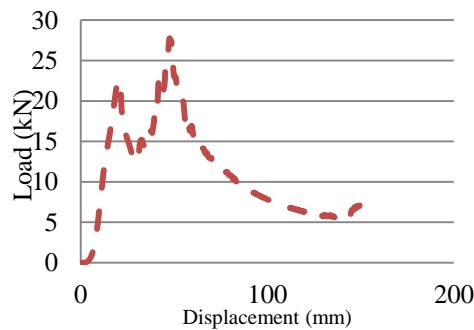
Model A1



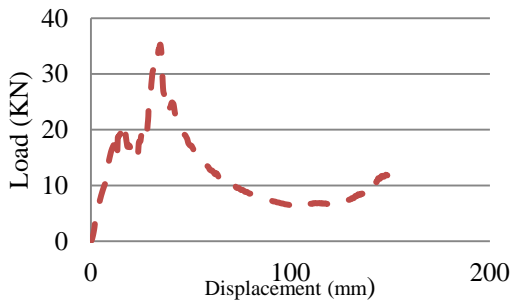
Model A2



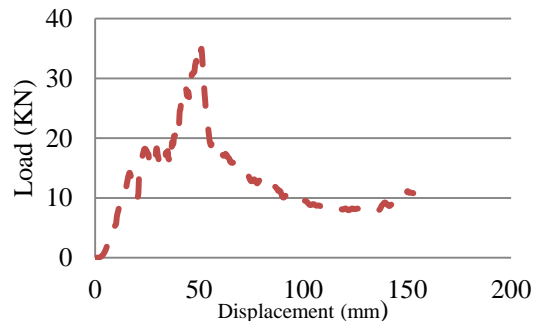
Model A3



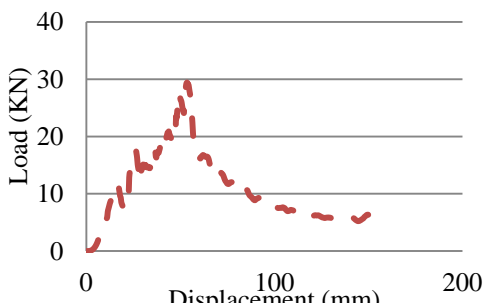
Model A4



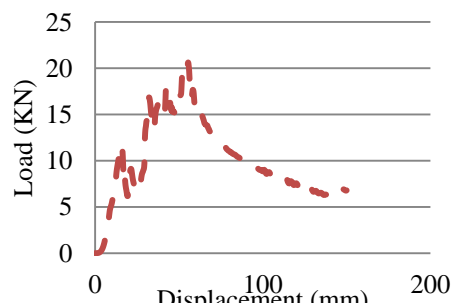
Model A5



Model A6



Model A7



Model A8

Fig5. Comparison of numerical load-displacement diagrams for different numerical test models

Fig6.

this end is fixed by a supporting frame of steel. This frame prevent the local collapse of the tubes and the load is totally applied as bending load, which results in domination of the bending collapse mode. While, in the present paper, models are not fixed by any supporting. In fact, they are directly in contact with the declined plate, thus the collapse mode starts locally from the point of contact. This boundary condition has more agreement to numerical results in reference [6]; however, there are some differences. According to reference [6]

by increasing the load angle, the dominant mode changes from the axial collapse to the bending which has also been indicated in the results of this paper. In the results of reference [6], this transition takes place in rather small load angles about  $7^\circ$ , while based on the present study, it is expected that the axial loading be the dominant mode even up to  $25^\circ$ . Seemingly, the important factor that influences on this angle is the friction between models and declined plate. The authors of reference [6] have neglected the friction between the declined plate and the tube; however, the present results show that due a great pressure between models and the declined plate, friction effects cannot be ignored. Obviously, in the absence of frictional resistance, the models will slide on the surface of the declined plate, and as a result the dominant mode becomes the bending mode

#### 4. Parametric study

In the following, to evaluate the effect of  $\theta_1$ ,  $\theta_2$  and  $C$  on the crushing behavior, a parametric study has been done using the FE model introduced the previous section. To this aim, 5 cases for  $C$  including:  $C=50, 55, 60, 65$  and  $70$  mm, and 4 cases for each of  $\theta_1$  and  $\theta_2$  equal to  $0, 15^\circ, 30^\circ$  and  $45^\circ$  were considered. Based on uniform combinations of these cases, a total number of  $4 \times 4 \times 5 = 80$  cases can be regarded. However, considering the fact that for  $\theta_2=0$ , all variations of  $\theta_1$  are identical, 15 cases from the all 80 ones are eliminated and eventually 65 different cases will remain. Figs. 6 to 9 represent the variation of energy absorption and peak crushing load based on  $\theta_1$  and  $\theta_2$  for different section widths. These diagrams provide the results of 65 different FE simulations performed using Abaqus program. For  $\theta_2=0^\circ$ , which specifically indicates the axial crushing, variation of  $\theta_1$  has no influence on the energy absorption, thus, the corresponding value is calculated

via modeling, and is further repeated four times in the diagrams.

As shown in Figs. 7 - 10, an increase in  $\theta_2$  considerably reduces the energy absorption as well as the peak crushing force, which signifies the importance of  $\theta_2$ . This can be attributed to this fact that by increasing  $\theta_2$ , the dominant mode changes from progressive buckling to the bending mode, and as a result, absorbed energy and maximum peak crush load decrease. Also, as seen in Figs. 7-10,  $\theta_1$  has significant effects on the crushing behavior of the tubes under 3D oblique loading. For instance, in Fig. 9, for  $C=50, 55$  mm and  $\theta_2=15^\circ$ ,  $\theta_1$  significantly changes the energy absorption which is mainly due to the transition in the collapse mode shape. Of course, by performing optimization process, one can acquire more precise results. Some intersections can be seen in a number of diagrams which can be attributed to the influence of  $\theta_1$  on the collapse mode shape, energy absorption and peak crushing load. For example in Fig. 7 for  $C=50$  mm, energy absorption has been considerably reduced for  $\theta_1=45^\circ$  and  $30^\circ$  with  $\theta_2=15^\circ$ .

It is deduced from the figures, as parameter  $C$  increases, particularly for  $C > 60$ mm, roughly lesser fluctuations in the absorbed energy can be seen by variations in  $\theta_1$ , especially for  $\theta_1=0^\circ, 15^\circ$ . Furthermore, for higher  $C$ , absorbed energy varies approximately with the same trend based on variations in  $\theta_2$ . As a result, by considering  $C > 65$  mm, a more reliable design can be achieved. It can now seem desirable to find a reliable value for  $\theta_1$  and  $\theta_2$  considering absorbed energy fluctuations. Evidently, larger  $\theta_1$  such as  $\theta_1=30^\circ, 45^\circ$  represent more robust, however, smaller energy absorption. But, for  $\theta_1=15^\circ$  and  $C > 60$ mm, a good behavior can be observed considering both of the above-mentioned criteria. As seen in Fig. 8, the trend for absorbed energy based on  $\theta_2$  remains almost identical for different  $\theta_1$  and  $C$ , however, a sharp decrease in the absorbed energy can be seen for  $\theta_2 > 30^\circ$ . So that the optimum values in terms of energy absorption for  $\theta_1$ ,  $\theta_2$  and  $C$  can be obtained equal to  $15^\circ$ , lower than  $30^\circ$ , and larger than  $60$ mm, respectively.

According to the figures, unlike absorbed energy, maximum peak crushing load ( $F_{max}$ ) shows very little fluctuations for different  $\theta_1$  and  $C$ . Evidently, for all calculated  $\theta_2$  except  $\theta_1=15^\circ$ , by increasing parameter  $C$ ,  $F_{max}$  experiences an increase. It is also seen that from  $\theta_1=0^\circ$  to  $\theta_1=15^\circ$ ,  $F_{max}$  has almost

decreased by 60%. As a result,  $\theta_1=15^\circ$  can be elected as an optimum value considering maximum peak

crushing load. As seen in Figs. 9 and 10, the trend of variation of  $F_{max}$  based on  $\theta_2$  for different  $C$  is.

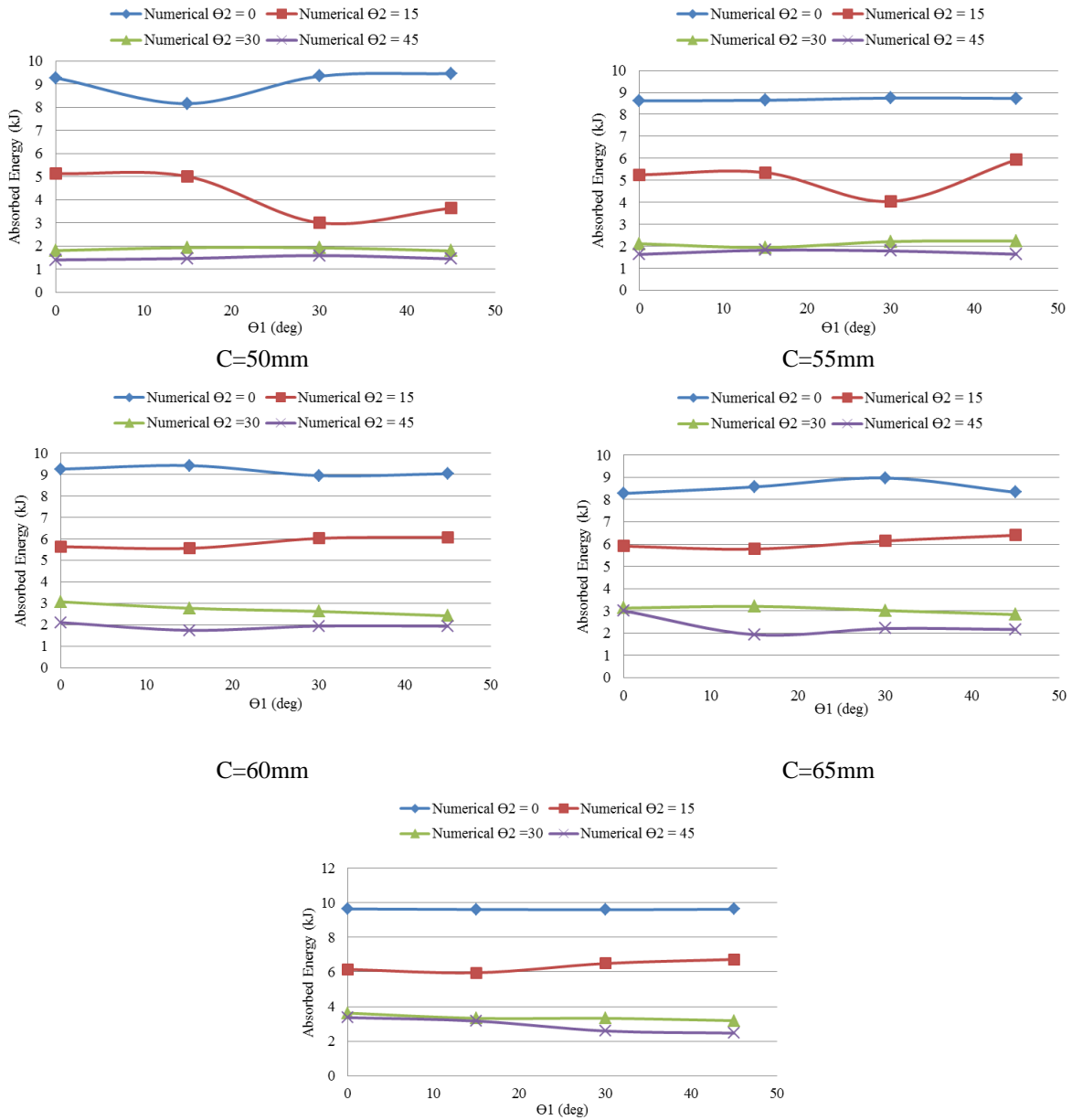


Fig7. Absorbed energy versus  $\theta_2$  for different tube widths (mm)

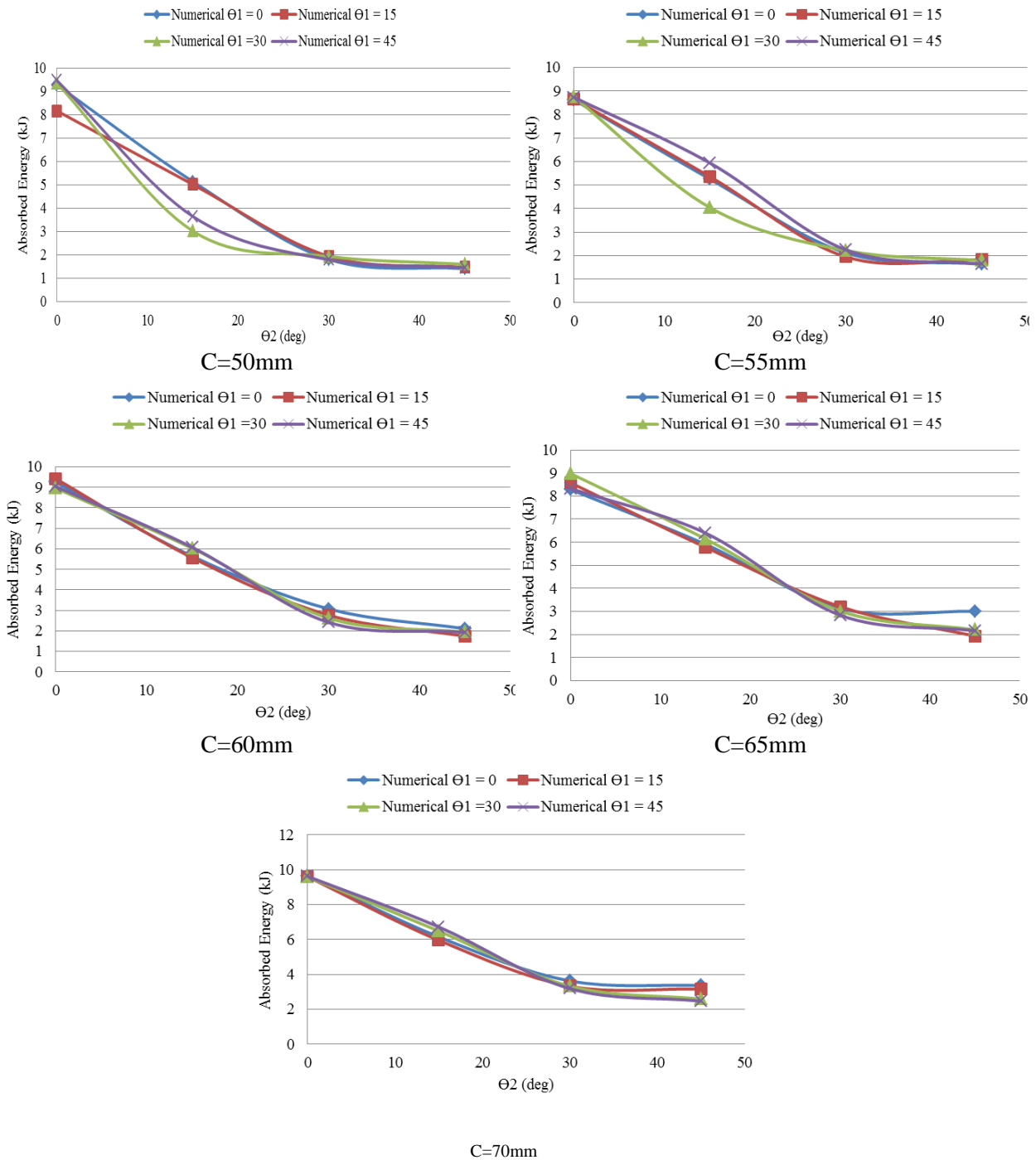


Fig8. Absorbed energy versus  $\Theta_2$  for different tube widths (mm)

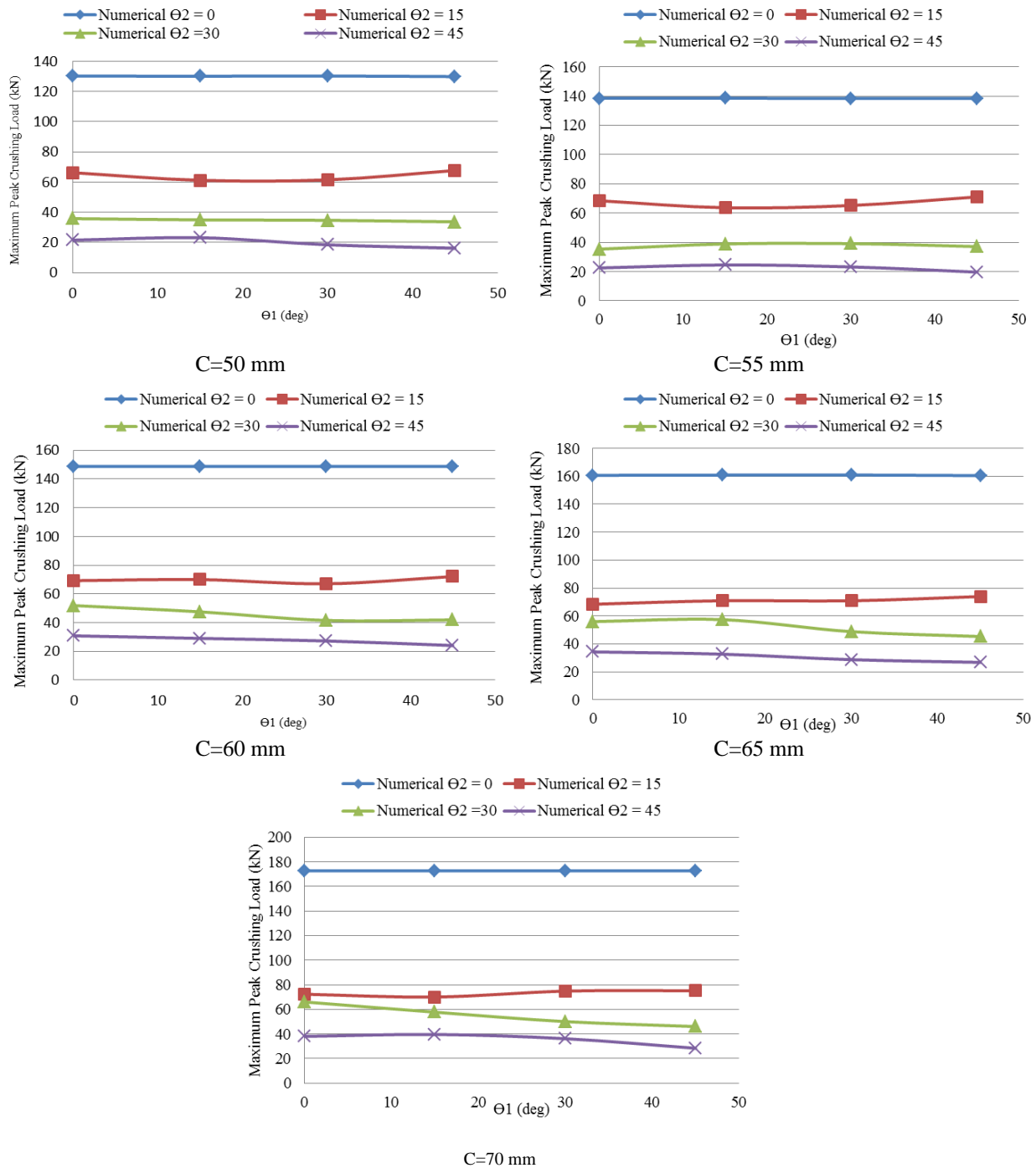


Fig9. Maximum peak crushing load versus  $\theta_1$  for different tube widths (mm)

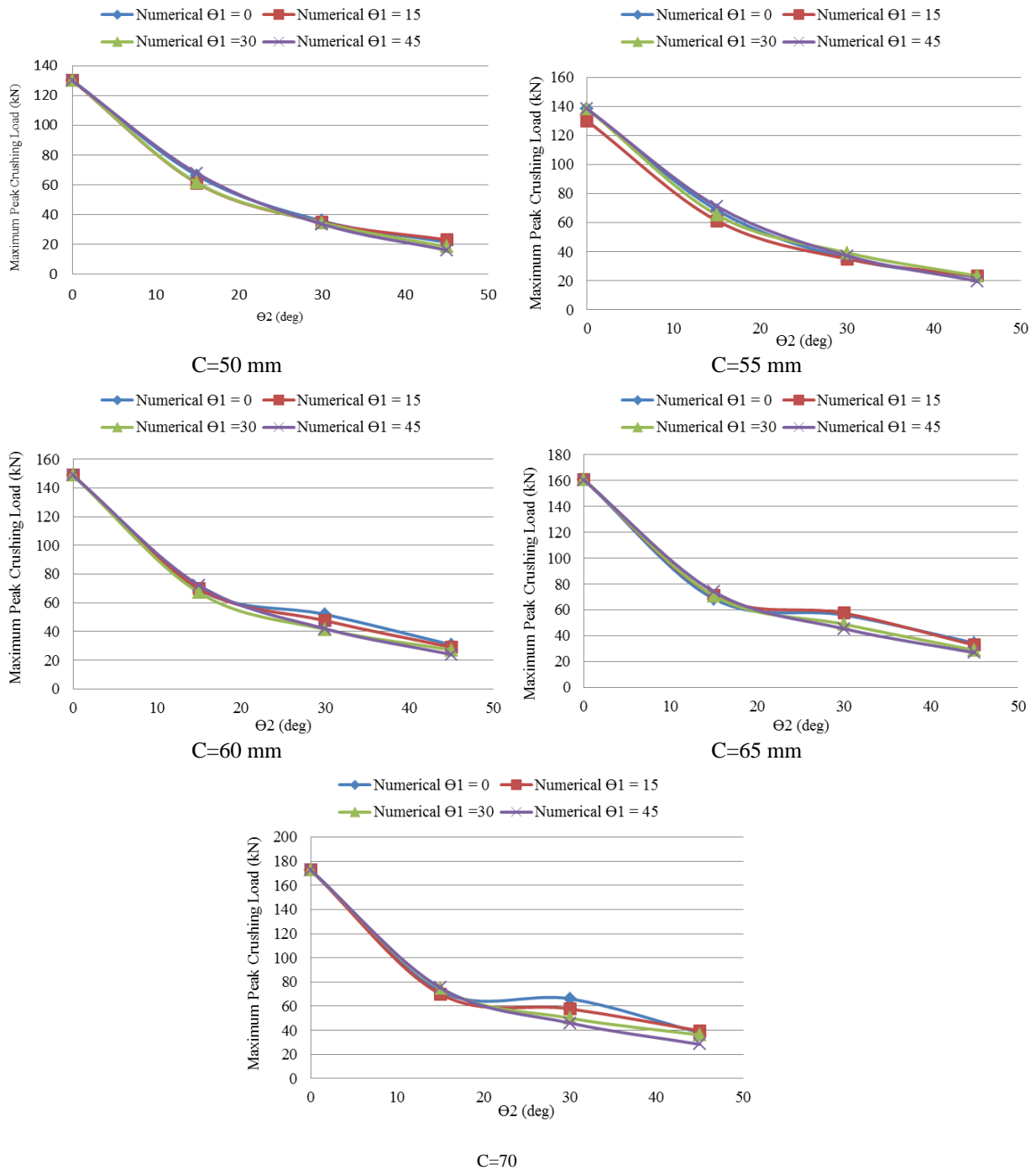


Fig10. . Maximum peak crushing load versus  $\theta_2$  for different tube widths (mm)

Identical, but for  $\theta_2 > 15^\circ$ ,  $F_{max}$  has dramatically fallen by increasing  $\theta_2$ . As a result, by considering the lowest maximum peak crushing load, optimum values for  $\theta_1$ ,  $\theta_2$  and  $C$  are  $15^\circ$ , larger than  $15^\circ$  as well as 50mm, respectively. By taking into account the optimum values previously obtained regarding best energy absorption, the best trade-off values for  $\theta_1$ ,  $\theta_2$  and  $C$  can be considered  $15^\circ$ , between  $15^\circ$  and  $30^\circ$ , as well as 60 mm, respectively. These optimum values can be used for many applications dealing with design of energy absorbers, particularly for vehicle s-rails

### Conclusions

Based on a more realistic approach towards crash events, 3D oblique loading, which is a new loading type in energy absorption studies, was introduced and its effects on the crushing behavior of thin-walled square tubes were investigated successfully. Subsequently, numerical simulations of quasi-static crushing of square tubes under oblique loading was carried out using FE method. It was proved that under 3D oblique loading, the crushing behavior is different from the conventional 2D oblique and axial loadings. Some important facts connected with the plastic collapse and deformation modes of thin-walled square tubes under 3D oblique loading were observed and discussed in details. Through parametric study, it was shown that defining angles of the 3D load have major effects on the load-displacement diagrams of thin-walled tubes.

## References

- [1]. Alexander JM, "An approximate analysis of the collapse of thin cylindrical shells under axial loading", *Quart. J. Mechs. and Applied Maths.* 1960; 13:1–9.
- [2]. Johnson W, Reid SR, "Metallic energy dissipating systems" *Applied Mechanics Review* 1978; 31(3):277–88.
- [3]. Jones N, Wierzbicki T, "Structural crashworthiness", London: Butterworth and Co. Publishers, 1983.
- [4]. Abramowicz W. The effective crushing distance in axially compressed thin-walled metal columns. *Int J Impact Engineering*; 13 (1983) 309-317
- [5]. Al Galib , D. Limam, A. Experimental and numerical investigation of static and dynamic axial crushing of circular aluminum tubes. *Thin-Walled Structures* 42 (2004) 1103–1137
- [6]. .D. C. Han, S. H. Park "Collapse behavior of square thin-walled columns under oblique loads", *J. Thin-Walled Structures*, 1999; 35,167-184.
- [7]. Reyes, A. Langseth, M. Hopperstad, O.S. Crashworthiness of aluminum extrusions under oblique loading: experiments and numerical analyses. *International Journal of Mechanical Sciences* 44 (2002) 1965–1984.
- [8]. A. Reyes, M. Langseth, O. S. Hopperstad "Square aluminum tubes under oblique loading", *International Journal of Impact Engineering* 28 (2003) 1077–1106.
- [9]. F. Tarlochan, F. Samer, A.M.S. Hamouda, S. Ramesh, "Karam Khalid, Design of thin wall structures for energy absorption applications: Enhancement of crashworthiness due to axial and oblique impact forces", *Thin-Walled Structures*, Volume 71, October 2013, Pages 7–17
- [10]. S.P Santosa, T. Wierzbicki, A.G. Hanssen, M. Langseth, Experimental and numerical studies of foam-filled sections, *Int. J. Impact Engineering*, 24 (2000) 509-534.
- [11]. V. Tarigopula, M. Lanseth, O.S. Hopperstad, A.H. Clausen, Axial crushing of thin-walled high-strength steel sections, *Int. J. Impact Engineering* 32 (2006) 847–882.
- [12]. G.M. Nagel, D.P. Thambiratnam, Dynamic simulation and energy absorption of tapered thin-walled tubes under oblique impact loading, *Int. J. Impact Engineering* 32 (2006) 1595–1620.
- [13]. Abolfazl Khakhalia, Nader Nariman-zadeh, A. Darvizeh, A. Masoumi and B. Notghi, "Reliability-based robust multi-objective crashworthiness optimisation of S-shaped box beams with parametric uncertainties", *International Journal of Crashworthiness*, Vol. 15, No. 4, August 2010, 443–456